A new proposal to Jefferson Lab PAC25

Measurements of Target Single-Spin Asymmetry in Elastic ep Scattering

D. Dutta, H. Gao, K. Kramer, X. Qian, X. Wang, Q. Ye, X. Zong
Duke University, Durham, North Carolina.

R. Gilman, C. Glashausser, X. Jiang (Co-Spokesperson) [a], G. Kumbartzki, K. McCormick, R. Ransome
Rutgers University, Piscataway, New Jersey.

A. Afanasev, D. Higinbotham, M. K. Jones (Co-Spokesperson), R. Michaels, B. Wojtsekhowski
Thomas Jefferson National Accelerator Facility, Newport News, Virginia.

P. Bosted (Co-Spokesperson), D. Lawrence, R. Miskimen, K. Paschke, G. A. Peterson, S. Rock
University of Massachusetts at Amherst, Amherst, Massachusetts.

D. Crabb (Co-Spokesperson), D. Day, B. Norum, O. Rondon, K. Wang
University of Virginia, Charlottesville, Virginia.

T. Averett
College of William and Mary, Williamsburg, Va.

Abstract

Abstract: We propose measuring the target single-spin asymmetry (A_y) in elastic $ep^{\uparrow} \to ep$ reaction at Hall C using a vertically polarized NH_3 target. The single-spin asymmetry A_y arises from the interference between the one-photon exchange and two-photon exchange amplitudes and is sensitive to the imaginary part of the two-photon exchange amplitude. Similar two-photon exchange effects may resolve the current discrepancy between the Rosenbluth separation and polarization transfer techniques used to measure the ratio of electric and magnetic proton form factors. Observation of significant two-photon exchange contributions will likely have implication for other precision experiments, such as measurements of $R = \sigma_L/\sigma_T$ in inelastic lepton scattering and the determination of the Coulomb Sum Rule.

The experiment will use an existing 2.5 T normal-conducting magnet, an existing ^4He refrigerator, and some new microwave components to provide an NH3 target with average polarization of about 38%. An unpolarized electron beam with energy 4.8 GeV will be rastered over the target surface. Elastic scattering from free protons will be isolated from inelastic scattering and

[a] Contact person, email: jiang@jlab.org

quasi-free scattering from the nitrogen in the target by detecting both the electron and proton in coincidence in a large solid angle lead glass array, built from existing blocks. The detector is left-right and up-down symmetric, allowing simultaneous measurements of A_y at $\pm 90^c irc$ relative to the polarization directions, which minimizes the systematic error due to luminosity fluctuations between opposite target polarization measurements. The primary measurements of A_y will be divided into four bins in the kinematic range $2.5 < Q^2 < 4.5$ GeV^2 and $67^\circ < \theta_e^{cm} < 96^\circ$, with projected statistical errors of 0.23% to 0.33% and an overall systematic error of about 0.1% on A_y. The theoretical predictions are in the several percent range at these kinematics, so the experiment will be definitive. Additional single-arm measurements at low Q^2 will be made using small-angle electrons (in a lead glass calorimeter) and wide-angle protons (in HMS), in a kinematic region where two-photon contributions are expected to be relatively small.

Contents

1 Introduction

For the past forty years, information on the nucleon and nuclei structure has been obtained through the study of form factors extracted from elastic electron scattering experiments. Following a well-established formalism, the assumption of the one-photon exchange approximation (Born approximation) allows the interpretation of experimental cross sections in terms of elastic (Dirac and Pauli) form factors. The validity of this approach is based on the assumption that the two-photon-exchange contribution is negligible. As more precision data on cross section and polarization observables becomes available from new facilities, the accuracy of the Born approximation turns out to be one of the major systematic unknowns limiting the interpretation of data.

In the case of the proton form factors, two sets of experimental data consistently yield very different results on the ratio $\mu_p G_{Ep}/G_{Mp}$, as shown in Fig. 1. While experiments [1] using the Rosenbluth method consistently yield $\mu_p G_{Ep}/G_{Mp} \approx 1$ up to $Q^2 \approx 6.0$ GeV^2, the Jefferson Lab recoil polarization data [2,3] demonstrated that G_{Ep}/G_{Mp} decrease quickly as a function of Q^2. A recent global reanalysis [4] of the cross section data found no inconsistency in the existing data sets. It was further confirmed that the apparent discrepancy cannot be removed by excluding any data set or modifying the relative normalization factors. To fully resolve the discrepancy, an error in the cross section data would have to introduce an ϵ-dependence of more than 5% for $Q^2 > 1.0$ GeV^2, which is an unlikely scenario to happen in every set of measurements. Confirming this discrepancy, preliminary results from the Jefferson Lab Hall A super-Rosenbluth experiment [5], and the Hall C E94-110 experiment [6] are in good agreement with the existing cross section data. The existence of this strong discrepancy indicates a fundamental flaw in one of the

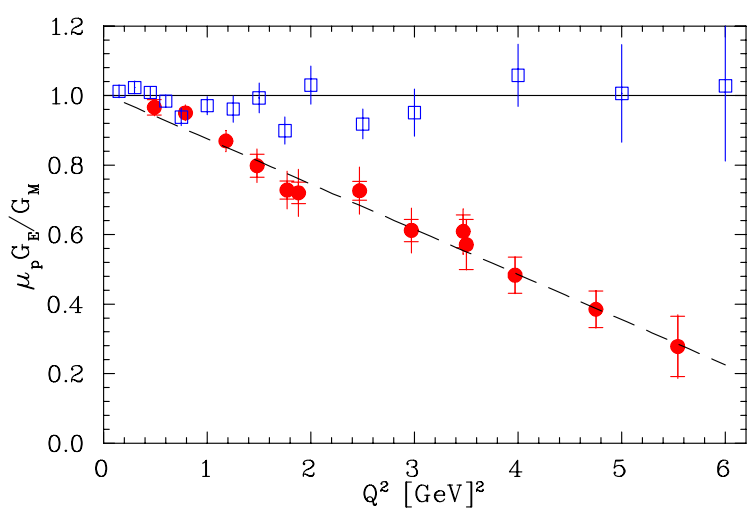

Figure 1: The existing data of $\mu_p G_E/G_M$ for proton [4] from recoil polarization measurements [2,3] (solid circles) and from cross section measurements [1] (open squares).

two experimental techniques, or a significant systematic error in either the recoil polarization or cross section measurements. The apparent discrepancy in G_{Ep}/G_{Mp} has recently been attributed to a possible failure of Born approximation at large Q^2 due to two-photon-exchange contributions[7,8]. One of the promising ways to explore the two-photon exchange mechanism in elastic electron-nucleon scattering is to observe the T-odd parity-conserving target single-spin asymmetry[9,10]. This single-spin asymmetry, A_y, is time-reversal odd, but A_y does not violate time-reversal invariance. It arises from the imaginary part of the interference between one- and two-photon exchange amplitudes, and it is related to the weighted integral of the off-forward extension of the virtual Compton scattering amplitude with two space-like photons[10]. Information about this amplitude cannot be obtained from other experiments and an extrapolation from the forward limit was used[10] based on present knowledge of t-dependence of GPDs in large-t real Compton scattering. With elastic intermediate state, A_y is expected to reach the level of one percent, the presence of intermediate resonance states between the two virtual photons might additionally enhance A_y as shown in Afanasev *et al.*.

Although the importance of observing A_y has been realized for many years, a non-vanishing A_y has never been clearly established in any experiment. In the late 1960s, A_y measurement[11] was among the first generation of SLAC experiments. With an incident electron beam of 15 and 18 GeV, A_y was observed to be consistent with zero up to $Q^2 = 0.98$ GeV^2 within the experimental accuracy of $1 \sim 2\%$, as shown in Fig. 2. However, a rather small A_y is expected ($A_y < 0.5\%$) at the SLAC kinematics[10] due to the very forward scattering angles, $2.4^\circ < \theta^e_{lab} < 3.2^\circ$ ($13.5^\circ < \theta^e_{cm} < 19.9^\circ$), since A_y is suppressed by a kinematic factor of $\sin\theta^e_{cm}$. The goal of this experiment is to

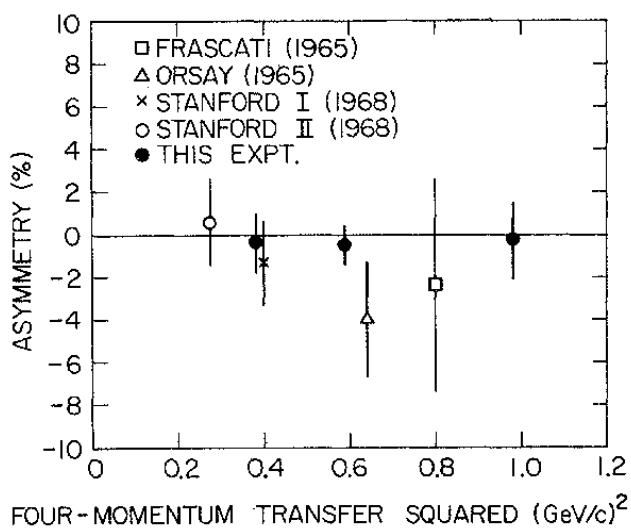

Figure 2: Data from the SLAC A_y measurements[11] referred to as "THIS EXPT." in the plot. Other data points are from measurements of the induced recoil polarization P_y. Time reversal invariance requires[9] that $P_y = A_y$.

make the first measurement of a non-vanishing A_y in elastic ep reaction, with statistical uncertainties of $0.23 \sim 0.33\%$. This experiment will measure A_y up to Q^2 of 4.5 GeV^2 at the electron's center-of-mass angle $67^\circ \sim 95^\circ$, for which the two-photon exchange effect is expected to produce a sizable single spin asymmetry. Taking advantage of the CW beam of CEBAF, this experiment will make coincidence measurement detecting both the scattered electron and the recoil proton. Moreover, A_y will be measured simultaneously using both $e+p$ type and $p+e$ type coincidence events within the same detector setup. This arrangement allows a built-in check of systematic uncertainties, since a physics asymmetry A_y changes sign between $e+p$ and $p+e$ measurements. Several independent methods are to be employed to determine the relative luminosities for target spin up and spin down runs. Special efforts are made to identify possible systematic uncertainties and false asymmetries.

It is important to establish the validity of two-photon calculations, not only to help resolve the G_{Ep}/G_{Mp} discrepancy, but also for the interpretation of all experiments involving precise cross section measurements, particularly when small cross section differences are used to separate transverse and longitudinal contributions. One example is the determination of the Coulomb Sum Rule, in which various experiments seem to disagree on whether the Sum Rule is satisfied or not. Another example is the determination of $R = \sigma_L/\sigma_T$ in inelastic lepton scattering. The statistical error on JLab measurements of R is now small enough that the effect of two-photon contributions may not be negligible.

2 Physics Motivation

2.1 Two-photon-exchange contribution in elastic ep scattering

In the framework of one-photon exchange approximation, two form factors appear in the matrix elements of the electro-magnetic current in elastic lepton-nucleon scattering: the magnetic (G_M) and the electric (G_E) form factors.

Experimentally, two independent methods had been used to determine the ratio of $R = \mu_p G_E/G_M$. The first method, the Rosenbluth method [14], is through the measurements of cross sections :

$$d\sigma_B = C_B(Q^2,\varepsilon)\left[G_M^2(Q^2) + \frac{\varepsilon}{\tau}G_E^2(Q^2)\right], \tag{1}$$

where $\tau = Q^2/4M^2$, ε is the photon polarization parameter, and $C_B(Q^2,\varepsilon)$ is a kinematic factor. For a fixed Q^2, one measures the cross section for different values of ε to determine the form factors G_M and G_E. The second method, the polarization method, is to measure the ratio of the recoil proton polarization perpendicular to its motion (P_t) to that along its motion (P_l) :

$$\frac{P_t}{P_l} = -\sqrt{\frac{2\varepsilon}{\tau(1+\varepsilon)}}\frac{G_E}{G_M}. \tag{2}$$

As shown in Fig. 1, the two sets of experimental data consistently yield very different results. It was pointed out that the discrepancy in G_E/G_M can be explained as a possible failure of the Born approximation when two-photon-exchange contributions are considered [7,8].

Under Lorentz, parity and charge conjugation invariance, the T-matrix for elastic scattering of two spin-1/2 particles can be expanded in terms of six independent Lorentz structures [15], three of them remain non-zero at the limit of $m_e \to 0$. Therefore, the T-matrix becomes :

$$T = \frac{e^2}{Q^2}\,\bar{u}(k')\gamma_\mu u(k)\cdot\bar{u}(p')\left(\tilde{G}_M\,\gamma^\mu - \tilde{F}_2\frac{P^\mu}{M} + \tilde{F}_3\frac{\gamma.KP^\mu}{M^2}\right)u(p), \qquad (3)$$

where $K = (k+k')/2$. $\tilde{G}_M$, $\tilde{F}_2$, $\tilde{F}_3$ are complex functions of ν and Q^2, and each contains information about nucleon structure. Under the Born approximation, one restores the relation :

$$\begin{aligned}\tilde{G}_M^{Born}(\nu,Q^2) &= G_M(Q^2),\\ \tilde{F}_2^{Born}(\nu,Q^2) &= F_2(Q^2),\\ \tilde{F}_3^{Born}(\nu,Q^2) &= 0,\end{aligned} \qquad (4)$$

where $F_2 = (G_E - G_M)/(1+\tau)$. Since $\tilde{F}_3$ and the phases of $\tilde{G}_M$ and $\tilde{F}_2$ vanish in the Born approximation, they must originate from processes involving at least the exchange of two photons, such as the box diagram in Fig. 3.

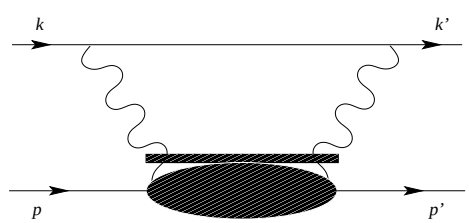

Figure 3: The box diagram of two-photon exchange, the filled ellipse represents the response of the nucleon to the scattering of the virtual photon.

The cross section and the recoil polarization are related to the real part of the two-photon-exchange amplitudes in different ways [7]:

$$\frac{d\sigma}{C_B(\varepsilon,Q^2)} \simeq \frac{|\tilde{G}_M|^2}{\tau}\left\{\tau + \varepsilon\frac{|\tilde{G}_E|^2}{|\tilde{G}_M|^2} + 2\varepsilon\left(\tau + \frac{|\tilde{G}_E|}{|\tilde{G}_M|}\right)\mathcal{R}\left(\frac{\nu\tilde{F}_3}{M^2|\tilde{G}_M|}\right)\right\}, \qquad (5)$$

$$\frac{P_t}{P_l} \simeq -\sqrt{\frac{2\varepsilon}{\tau(1+\varepsilon)}}\left\{\frac{|\tilde{G}_E|}{|\tilde{G}_M|} + \left(1 - \frac{2\varepsilon}{1+\varepsilon}\frac{|\tilde{G}_E|}{|\tilde{G}_M|}\right)\mathcal{R}\left(\frac{\nu\tilde{F}_3}{M^2|\tilde{G}_M|}\right)\right\}, \qquad (6)$$

where $\mathcal{R}$ denotes the real part, and $\tilde{G}_E = \tilde{G}_M - (1+\tau)\tilde{F}_2$.

The size of the real part of 2γ-contribution $Y_{2\gamma} = \mathcal{R}(\nu\tilde{F}_3/M^2|\tilde{G}_M|)$ was determined to be at the order of a few percent, as shown in Fig. 4, by fitting

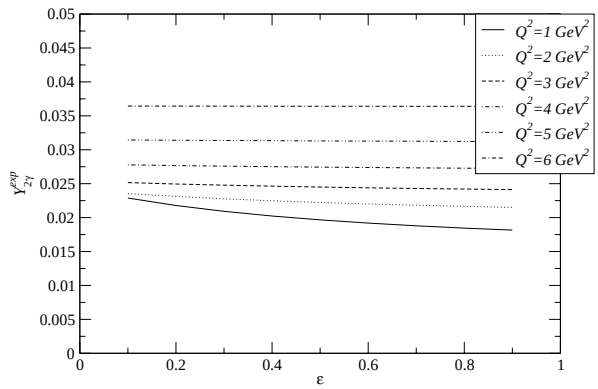

Figure 4: The size of the real part of the two-photon-exchange contribution $Y_{2\gamma}$ as determined in Ref. [7].

the experimental data and assuming the two-photon-exchange contribution alone causes the G_{Ep}/G_{Mp} discrepancy.

A calculation which includes only the nucleon intermediate state found that the two-photon-exchange correction has the proper sign and the magnitude to resolve a large part of the discrepancy [8], as shown in Fig. 5.

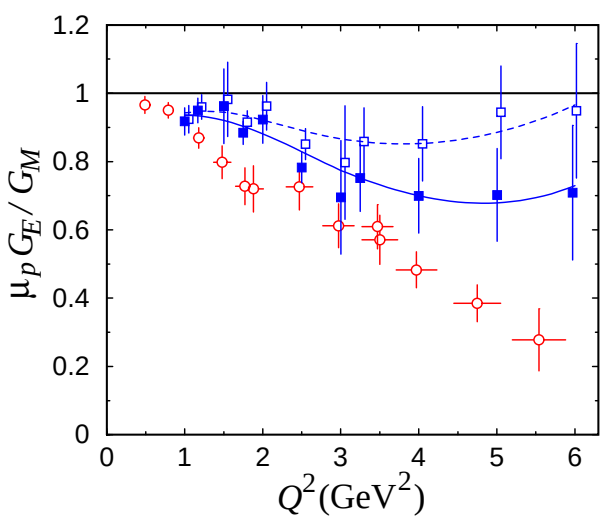

Figure 5: Data for the $\mu_p G_E/G_M$ from Rosenbluth separation measurements with no two-photon corrections (open blue squares) and with a calculated two-photon correction including only the nucleon intermediate ground state [8].

2.2 Target single-spin asymmetry A_y

An observable which is directly proportional to the two- (or multi-) photon exchange is given by the elastic scattering of an unpolarized electron on a proton target polarized normal to the scattering plane (or the recoil polarization normal to the scattering plane, which is exactly the same assuming

time-reversal invariance).

$$A_y = \frac{\sigma_\uparrow - \sigma_\downarrow}{\sigma_\uparrow + \sigma_\downarrow}, \tag{7}$$

where $\sigma_\uparrow$ ($\sigma_\downarrow$) denotes the cross section for an unpolarized beam and for a nucleon spin parallel (anti-parallel) to the normal polarization vector. As has been shown by de Rujula *et al.*, the target (or recoil) normal spin asymmetry is related to the absorptive part of the elastic eN scattering amplitude. Since the one-photon exchange amplitude is purely real, the leading contribution to A_y is of order $O(e^2)$, and is due to an interference between one- and two-photon exchange amplitudes.

When neglecting terms which correspond with electron helicity flip (i.e. $m_e = 0$), the general expression for A_y can be expressed in terms of the invariants for electron-nucleon elastic scattering as :

$$A_y = \sqrt{\frac{2\,\varepsilon\,(1+\varepsilon)}{\tau}}\;\frac{C_B(\varepsilon, Q^2)}{d\sigma}\;\left\{\mathcal{I}\left(\tilde{G}_M\,\tilde{G}_E^*\right) + \rho\mathcal{I}\left(\left(\tilde{G}_M - \frac{2\,\varepsilon}{1+\varepsilon}\tilde{G}_E\right)\tilde{F}_3^*\right)\right\}, \tag{8}$$

where $\mathcal{I}$ denotes the imaginary part. We immediately see that A_y vanishes in the Born approximation, and is therefore of order e^2. Eq. (8) can be simplified by keeping only the leading term of order e^2. To this order, A_y arises from an interference between the one- and two-photon exchange amplitudes and is given by :

$$\begin{aligned} A_y = & \sqrt{\frac{2\,\varepsilon\,(1+\varepsilon)}{\tau}}\;\left(1 + \frac{\varepsilon}{\tau}\frac{|\tilde{G}_E|^2}{|\tilde{G}_M|^2}\right)^{-1} \\ & \times\left\{\frac{|\tilde{G}_E|}{|\tilde{G}_M|}\phi_{ME} - \left(1 - \frac{2\,\varepsilon}{1+\varepsilon}\frac{|\tilde{G}_E|}{|\tilde{G}_M|}\right)\mathcal{I}\left(\frac{\nu\tilde{F}_3}{M^2|\tilde{G}_M|}\right)\right\}. \end{aligned} \tag{9}$$

The single spin asymmetry A_y measures the imaginary part of $\tilde{F}_3$, offset by the phase difference ϕ_{ME} between the amplitudes $\tilde{G}_M$ and $\tilde{G}_E$. If one naively assumes the real and the imaginary parts of two-photon-exchange amplitude are of the same order, $\mathcal{I}(\tilde{F}_3) \approx \mathcal{R}(\tilde{F}_3)$, A_y can be significantly larger than 1%.

2.3 Existing data

In the late 1960s, several experiments were carried out for measurements of both target single-spin asymmetry A_y and the induced proton recoil polarization P_y in elastic ep reaction up to Q^2 of 1.0 GeV^2. Both A_y and P_y were found to be consistent with zero within the large statistical uncertainties, as shown in Fig. 2.

An experiment at Stanford in 1968 measured the ratio of positron-proton to electron-proton elastic cross sections [16]. This charge-conjugation odd cross section difference, $\sigma^+ - \sigma^-$, is related to the real part of one- and two-photon interference amplitudes. At $Q^2 > 2.0$ GeV^2, data were consistent with identical cross sections within the large statistical uncertainties, as shown in Fig. 6.

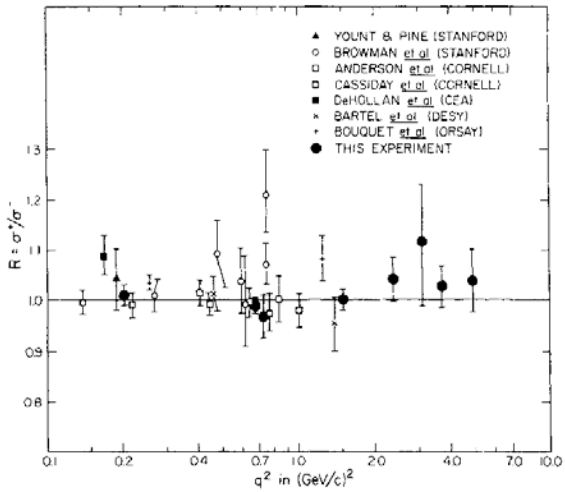

Figure 6: Measurements of the ratio of e^+p to e^-p elastic scattering as a function of Q^2. The high Q^2 SLAC measurements [16] referred to as "THIS EXPERIMENT" in the plot.

3 The Proposed Experiment

We plan to measure the target single-spin asymmetry A_y in Jefferson Lab Hall C using a vertically polarized NH_3 target and a 4.8 GeV unpolarized electron beam. Beam polarization is not a concern in this experiment. Two sets of detectors centered at 30.75° on each side of the beam will collect both $e+p$ and $p+e$ coincidence events simultaneously, as illustrated in Fig 7. The built-in cross-check of $A_y^{ep} = -A_y^{pe}$ serves as a clear measure of systematic uncertainties.

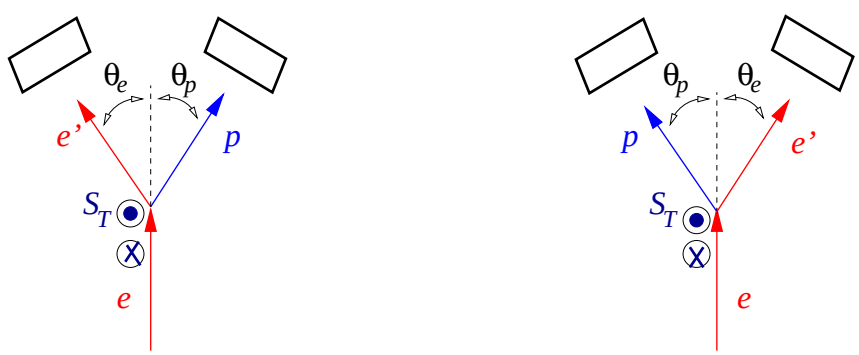

Figure 7: The schematic view of the A_y measurement. Both $e+p$ (left) and $p+e$ (right) coincidence events will be collected simultaneously using the same detectors.

Coincidence $p(e, e'p)$ events count asymmetries, corrected by the measured relative-luminosities, will be formed corresponding to the target spin up and spin down runs. The target field will be kept in the same direction throughout the experiment. The target polarization direction will be reversed once every six hours by changing the target RF frequencies. There should be no correlation between the relative detection efficiency and the target RF frequency

changes. The relative beam charge of $Q_\uparrow/Q_\downarrow$ will be determined by the regular Hall C beam charge monitors. The relative stability of these charge monitors should be very reliable, especially since the stability will be independent of the target RF frequency changes. The relative luminosities, however, cannot be uniquely determined by the relative beam charge. Therefore, reliable luminosity monitors are needed for this experiment.

Downstream luminosity monitor units, positioned above and below the beam pipe at 5° and 10° scattering angles, will count high energy electrons from the target to provide a continuous record of the relative luminosities. In addition, around the 10° scattering angle cone downstream of the target, four other calorimeter units will collect high energy electrons to perform independent single-arm A_y measurements at $Q^2 = 0.65$ (GeV/c)^2 from four different azimuthal angles. Further more, the HMS will detect low Q^2 single-arm elastic proton events at a scattering proton angle of 70.43° .

3.1 Kinematics

We chose to measure A_y at the highest possible Q^2 at which the event rate still allows for a reasonable statistical accuracy. The choice of kinematics is determined by two considerations. Guided by theoretical predictions, the largest A_y is expected at center-of-mass angles around 90° . In addition, at $\theta_{cm} \approx 90°$, the scattered electron and the recoil proton have similar momentum and lab angles such that both $e + p$ and $p + e$ events can be detected simultaneously in the same detector setup.

For $E_0 = 4.8$ GeV, the two detector arrays will be centered at 30.75° on the opposite side of the beam. The central kinematics for each Q^2 bin, the corresponding rates for $e + p$ and $p + e$ events are listed in Table 1. The expected total statistical uncertainties of A_y measurements are also listed. The rates and error estimation are based on a 360 hour measurement using a 5 cm NH_3 target and a 50 nA beam with an average target polarization of 0.38 and a dilution factor of $\eta = 0.9$. The rates are obtained within the coincidence phase space through a detailed Monte Carlo simulation which includes detector geometry and the target magnetic field.

3.2 Main set of two pairs of calorimeters

Given the limited luminosity that the polarized NH_3 target can tolerate, the only practical method for reducing the statistical error of this experiment is to maximize the solid angle of the detectors. The experiment takes advantage of the fact that the elastic *ep* reaction can be kinematically isolated using the angular correlation between the scattered electron and proton. Therefore, if the scattering angles can be measured with sufficient accuracy, then momentum resolution of the detector is not a critical concern. Based on these considerations, we choose to use lead-glass calorimeters with good granularity and reasonable energy resolution. Since we intend to directly compare measurements of A_y from $e + p$ and $p + e$ events, the calorimeters will be used to

E_0 GeV	$\langle Q^2 \rangle$ GeV^2	E' GeV	θ_e deg	p_p GeV/c	θ_p deg	θ_e^{cm} deg	ep-rate per day	pe-rate per day	δA_y %
4.80	2.50	3.47	22.35	2.07	39.61	67.01	47 k	62 k	0.23
	2.95	3.23	25.20	2.33	36.19	73.67	49 k	54 k	0.23
	3.45	2.96	28.50	2.61	32.77	80.80	56 k	55 k	0.23
	4.50	2.40	36.40	3.20	26.44	95.55	27 k	24 k	0.33
detector center:			30.75		30.75				

Table 1: Kinematics and count rates for each Q^2 bins. Data for all Q^2 bins are taken at the same time. θ_e is the initial angle of the scattered electron, θ_p is the initial angle of the recoil proton. The total statistical uncertainty δA_y is for a 360 hour measurement which takes into account both $e+p$ and $p+e$ events.

detect electrons and protons at the same time and are designed to be similar on both sides of the beam line.

Four nearly identical lead-glass calorimeters would be built from the lead-glass used in the BigCal calorimeter. The calorimeter array, BigCal, combines lead-glass blocks used in the Hall A Real Compton experiment and lead-glass from the Protvino group that was used at Fermilab. Each RCS lead-glass block has a 4x4 cm cross-section and length of 40 cm, while the Protvino lead-glass block has 3.8x3.8 cm cross-section with a length of 45 cm. The lead-glass is already stacked 218 cm in height x 120 cm in width. The blocks are individually wrapped with a thin layer of 1 mil thick aluminized mylar,so they are optically isolated from each other. The electron energy resolution is expected to be $5\%/\sqrt{E(\mathrm{GeV})}$. A horizontal and vertical position can be determined by the energy-weighted centroid of the cluster of blocks which share the energy and the uncertainty is expected to be < 0.5 cm.

For this experiment, the lead-glass from the BigCal calorimeter would be arranged into four separate detectors. Each detector would cover a width of about 84 cm (22 Protvino blocks or 21 RCS blocks) and a height of about 76 cm (20 Protvino blocks or 19 RCS blocks). Two calorimeters would be on the beam left and two would be on the beam right. Each would be at an angle of 30.75° and the front face would be a distance of 230 cm from the target center. On each side of the beam, a calorimeter would be placed above and below the beam line. Each calorimeter module will be centered at ± 46.4 cm realtive to the beam line, leaving a gap of 16.8 cm between the upper and lower modules. The maximum Cartesian out-of-plane angle is about 20° which is within the acceptance allowed by the target magnet pole faces.

In Fig. 8, the x versus y position at the calorimeters in plotted for $e+p$ reaction (e is detected by beam left calorimeter and p is detected by beam right calorimeter). While, in Fig. 9, the x versus y position at the calorimeters in plotted for $p+e$ reaction (p is detected by beam left calorimeter and e is detected by beam right calorimeter).

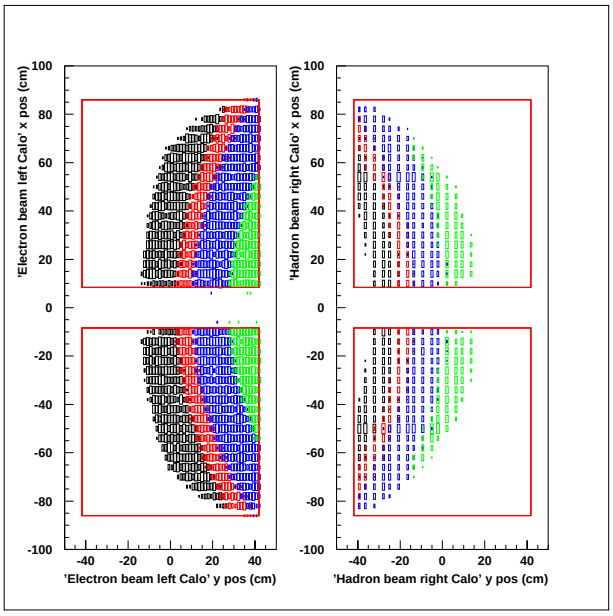

Figure 8: Plots of the x versus y position at the calorimeters for elastic $e + p$ reaction. *Left*: The beam left calorimeters which detects es. *Right:* The beam right calorimeters which detects ps . The color code is explained in the text.

Both sets of figures have the following features. The x-direction is the vertical direction with $+x$ in the downward direction. The y-direction is the horizontal direction with $+y$ pointing to smaller angles for the beam right calorimeter and $+y$ pointing to larger angles for the beam left calorimeter. The plots are from a Monte Carlo explained later in the proposal. Each color band is a different Q^2 region. The data are divided into Q^2 regions centered at $Q^2 = 2.5$, 2.95, 3.45, and 4.5 GeV^2 (color coded: black, red, blue and green, respectively). The red boxes in the plots are the physical dimensions of the calorimeters.

For the $e+p$ reaction, the electron and proton are bent towards to beamline so that they both cover the small angle side of the calorimeters. While for the $p + e$ reaction, the electron and proton are bent away from beamline so that they both cover the large angle side of the calorimeters.

A GEANT simulation was performed to investigate the detector's response to a 2.75 GeV/c proton. The simulation includes air gaps and mylar wraps around the blocks. A large fraction of the protons will deposit 200 MeV energy due to dE/dx while a considerable fraction of protons deposit more than 200 MeV in total energy. The total energy deposit over a 3-block by 3-block area is shown in Fig. 10 (left). The proton hit cluster size is also studied through the simulation. When requiring a hit carries more than 20 MeV energy deposit, the cluster size peaks at 1-block for head on tracks, and $2 \sim 3$-blocks for tracks that come in at $5°$. The result of cluster size simulation is shown in Fig. 10 (right).

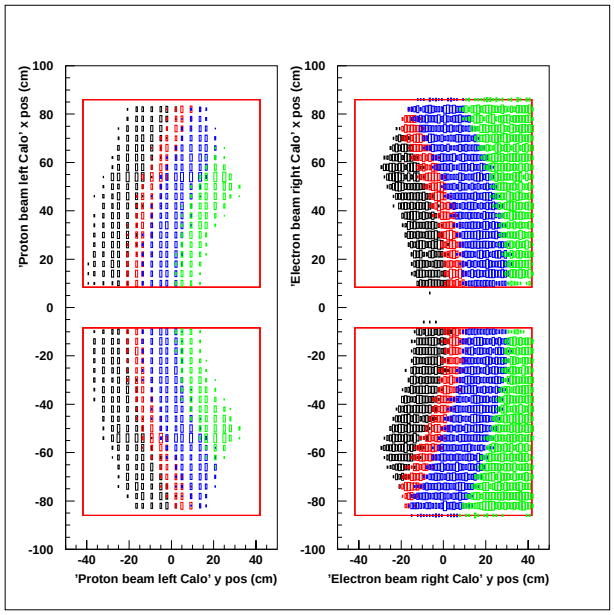

Figure 9: Plots of the x versus y position at the calorimeters for elastic $p + e$ reaction. *Left*: The beam left calorimeters which detects protons. *Right:* The beam right calorimeters which detects electrons . The color code is explained in the text.

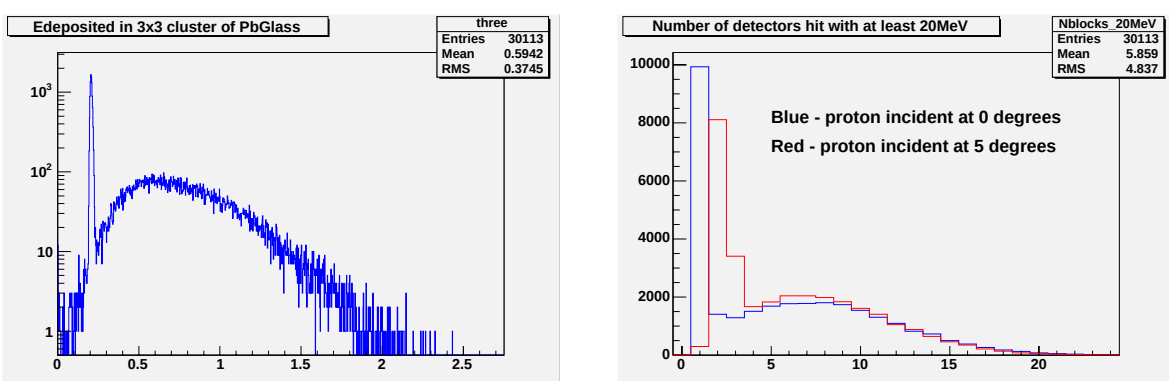

Figure 10: GEANT simulation results for $p_p = 2.75$ GeV/c proton on the lead-glass array. The total energy deposit over 3-block by 3-block area is on the left, the proton hit cluster size is on the right

3.3 Trigger and DAQ

For the calorimeter, the analog signals from the individual blocks will be summed in groups of eight to produced a summed signal plus the individual analog signals are passed through to an ADC. The summed analog signal will be sent to a discriminator and a threshold equivalent to depositing 500 MeV in the calorimeter will be set. This logical signal will be sent to a TDC. The Rutgers University group is currently building the summing modules that will be used in BigCal for the Hall C G_{Ep} experiment. The BigCal calorimeter is also expected to be used in several other experiments in Hall C and Hall A.

3.4 The luminosity monitors and the measured asymmetry $\mathcal{A}_{measured}$

Experimentally, target single-spin asymmetry A_y is only related to the relative yields between target spin up ($\uparrow$) and spin down ($\downarrow$) configurations. Knowledge of acceptances, absolute detection efficiencies and absolute luminosities are not necessary. The measured single-spin asymmetry $\mathcal{A}_{measured}$ can be formed form the number of coincidence events (N), corrected by the relative luminosities ($\mathcal{L}$) corresponding to target spin up and spin down runs.

$$\mathcal{A}_{measured} = \frac{\frac{N_\uparrow}{\mathcal{L}_\uparrow} - \frac{N_\downarrow}{\mathcal{L}_\downarrow}}{\frac{N_\uparrow}{\mathcal{L}_\uparrow} + \frac{N_\downarrow}{\mathcal{L}_\downarrow}} \tag{10}$$

At 3.0 meters downstream of the target, symmetrically positioned around the primary beam direction, eight units of Lead-Fluoride calorimeter arrays (Lumi units) will be installed in a configuration as shown in Fig. 11 (left). Six Lumi units will be at locations corresponding to a 10° scattering angle, and two Lumi-units will be at a 5° scattering angle. The 128 calorimeter blocks, the complete electronics and readout system will be borrowed from the Hall A DVCS experiments, after the completion of the scheduled data taking in late 2004. There are 148 blocks available. The Rutgers University group will extend its role in the Hall A DVCS experiments and take the responsibility for the installation, calibration and operation of the downstream Lumi units for this experiment. A support structure to hold the Lumi units is to be built. To reduce the room background, helium bags will replace the narrow sections of the regular Hall C downstream beam pipe up to 1.0 meter beyond the Lumi units.

Each Lumi-unit contains 16 blocks, 3 cm×3 cm×18.4 cm each in a 4×4 arrangement, covering an area of 144 cm^2. These Lead-Fluoride blocks had been known to tolerate a much higher radiation environment, in the Hall A DVCS experiments these blocks will be used at 16° with a luminosity two orders of magnitude higher than this experiment. Exposing the crystals to UV light for 10 minutes has been found to completely recover any radiation damage. A small piece of scintillator, 6 cm×6 cm in size, covers the central four blocks to provide a gate whenever a charge particle hits. The Lumi units

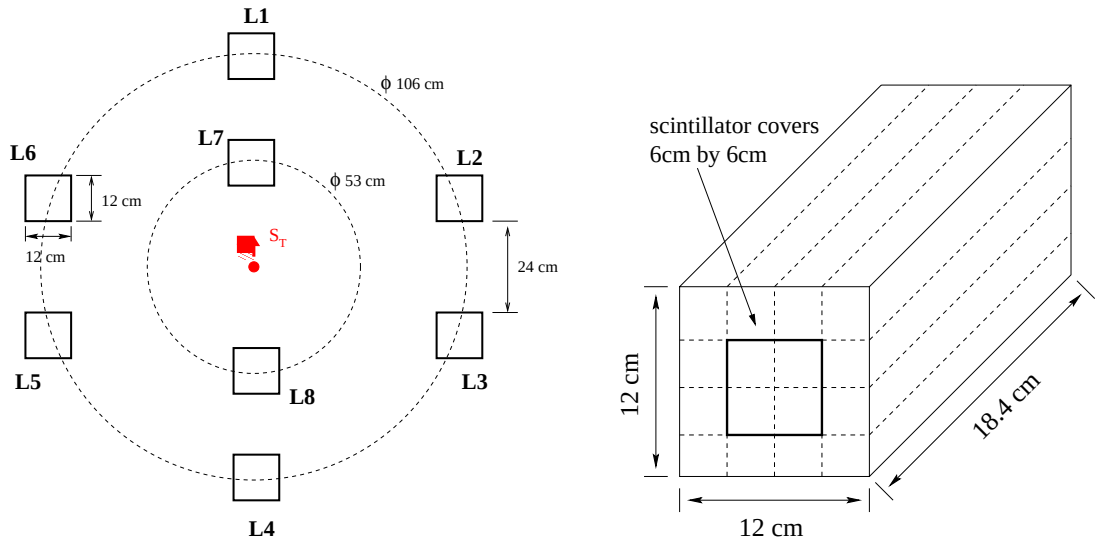

Figure 11: Left: the arrangement of eight luminosity monitor units at 3 meters downstream of the target. Units L1-L6 are corresponding to 10° scattering angle, units L7 and L8 are corresponding to 5° scattering angle. Right: each Lumi unit has 16 Lead-Fluoride blocks, a scintillator in the front covers the area of the central 4 blocks.

count only high energy charged particles passing through its central region. The trigger of the Lumi will be set to a very high energy threshold, 3.5 GeV for the 10° Lumi-units and 4.0 GeV for the 5° Lumi-units while a charged gate is present. The scaler and ADC information of each block will be readout for offline analysis.

The central four blocks of a Lumi unit cover a solid angle of 0.4 msr. The elastic $p(e, e')$ peak, or the center of the quasi-elastic $N(e, e')$ kinematics is listed in Table 2, together with the expected rates. Although energy resolution and the absolute energy calibration are not critical for the propose of luminosity monitoring, an energy resolution of 2.6% at 4.0 GeV has been demonstrated for a 3×3 unit in a Hall A test run. Since the electrons from Δ-production carry 7% less energy, separation between the elastic peak and the resonance peaks should be reasonable. This separation allows luminosity cross checks using electrons from different kinematic regions.

E_0 GeV	$\langle Q^2 \rangle$ GeV^2	E' GeV	θ_e deg	θ_e^{cm} deg	$\Delta\Omega_e$ msr	rates on NH_3 Hz
4.80	0.17	4.71	5.0	16.65	0.40	6 k
	0.65	4.45	10.0	32.68	0.40	100

Table 2: The rates on NH_3 and kinematics for each unit of the downstream electron monitors

The Lumi units L1, L7, L8 and L4 are in the same plane formed by the incoming electron and the target spin with $(\vec{e} \times \vec{e'}) \cdot \vec{S}_T \approx 0$, as illustrated in

Fig. 12. Any process that carries a non-vanishing single-spin asymmetry in this direction violates either time-reversal invariance or parity, which should be much below the level of 10^{-3}. In addition, most of the high energy particles that hit these units are coming from electrons quasi-elastically scattered off nitrogen nuclei, which are hardly polarized to start with. Therefore, counts of high energy particles from these units can be used to monitor the relative luminosity for target spin-up and spin-down runs. The exact position of these units are not relevant, since only the relative counts from the same units are needed.

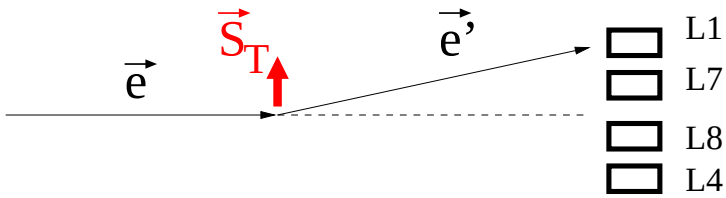

Figure 12: The Lumi units L1, L7, L8 and L4 are in the same plane as the incoming electron and the target polarization.

The 10° Lumi units L1 and L4 will be used as the primary luminosity monitors while units L7 and L8 will be used to cross check for stabilities of other units. The scattered electrons that hit Lumi units L2, L3, L5 and L6 might carry a small single-spin asymmetry to start with, since $(\vec{e} \times \vec{e'}) \cdot \vec{S}_T \neq 0$ for these units. However, the elastic asymmetry A_y is expected to be small and events from nitrogen quasi-elastic scattering will dilute the physics asymmetry. Should a non-zero asymmetry be consistently observed in these units, with same signs between L2 and L3 (L5 and L6) but opposite signs between L2 and L5 (L3 and L6), a non-vanishing A_y can be firmly established for $Q^2 = 0.65$ GeV^2 and $\theta_e^{cm} = 32.7°$.

3.5 Measurement at low Q^2 from proton singles

Simultaneous with the main measurement, the HMS (at 55.4° floor angle beam right) will be set to the central momenta of 0.57 GeV/c to detect the elastic single-proton events, as well as quasi-elastic $N(e,p)$ events. The kinematics and rates are listed in Table 3. This arrangement corresponds to the elastic scattering of $Q^2 = 0.3$ GeV^2, and $\theta_e^{cm} = 20°$ and $\theta_p = 70.44°$. About 10 million single proton elastic events will collect over the 360 hour measurement, resulting in a statistical uncertainty on δA_y of about 0.16%. At this kinematics, since the raw target single-spin asymmetry is expected to be less than 0.07%, single-proton measurement can be used effectively as additional luminosity monitor.

3.6 Singles rates and accidental coincidence events

To estimate the singles rates in each detector section, a Monte Carlo simulation [17] which includes the effects of target field, target geometry of detector

E_0 GeV	Q^2 GeV^2	p_p GeV/c	θ_p-initial deg	θ_e^{cm} deg	$\Delta\Omega_p$ msr	rates on NH_3	time hours	δA_y %
4.80	0.30	0.57	70.44	20.04	6.0	7.5 Hz	360	0.16

Table 3: Kinematics of the single-arm proton elastic ep scattering by the HMS spectrometer. The expected total statistical uncertainty on A_y is estimated assuming a target polarization of $P_T = 0.38$ and a dilution factor of $\eta_p = 0.5$.

geometry, heat shield and vacuum window materials was developed based on a well tested code of Jefferson Lab's radiation group.

The strong 2.5 T downward vertical target field bends low energy charged particles in the horizontal plane, causing a high flux of low energy electrons to beam-right and positrons to beam-left. However, Monte Carlo simulations indicate that ± 5.0 cm away from the horizontal plane, the flux of low energy particles drops significantly. To avoid radiation damage to the detectors, we chose to leave a horizontal gap of ± 16.8 cm between pairs detector on each side of the beam line.

The background singles rates of electron, positron and photon for the right-side and left-side detectors are plotted in Fig. 13. Rates of other types of particles are much less significant. The integrated rates (in cm^{-2}s^{-1}) above an energy threshold T are plotted as a function of the threshold T (MeV) in Fig. 13. The worst case of accidental rate will be in the $e+p$ type event selection of which a proton that hits on the beam right detector needs to be selected amid the background of low electrons. The right detector will experience a rate of 40 kHz/cm^2 for $T > 20$ MeV particles (140 kHz for $T > 0.1$ MeV). Over one section of 86 cm$\times$76 cm, 26 hits will be registered with $T > 20$ MeV (91 hits for $T > 0.1$ MeV) within a 100 ns time window of each trigger. Once a 5 ns flight time cut is applied offline, a factor of 10 accidental reduction is expected. A true proton-hit should deposit a total energy of 300 MeV in a hit-cluster on an average with at least one block receives more than 50 MeV. Therefore, for the worst case, no more than 2 accidental candidates per trigger over the entire detector section need further analysis. An additional requirement on co-plane geometry will eliminate accidental candidates by another factor of 100. An extra cut on calorimeter energy, corresponding to a cut at W $\approx$ 1.3 GeV, can also be used to further eliminate the accidental events.

3.7 The polarized NH_3 target

The single-spin asymmetry A_y is proportional to the component of the target polarization that is normal to the scattering plane, i.e.: $A_y \propto (\vec{e} \times \vec{e'}) \cdot \vec{S}_T$. Therefore, a maximum out-of-plane target polarization is preferred in order to have a significant measurement. The existing Hall C super-conducting polarized target magnet can only provide in-plane transverse polarization. The geometry of the existing target magnet coils excludes options of putting

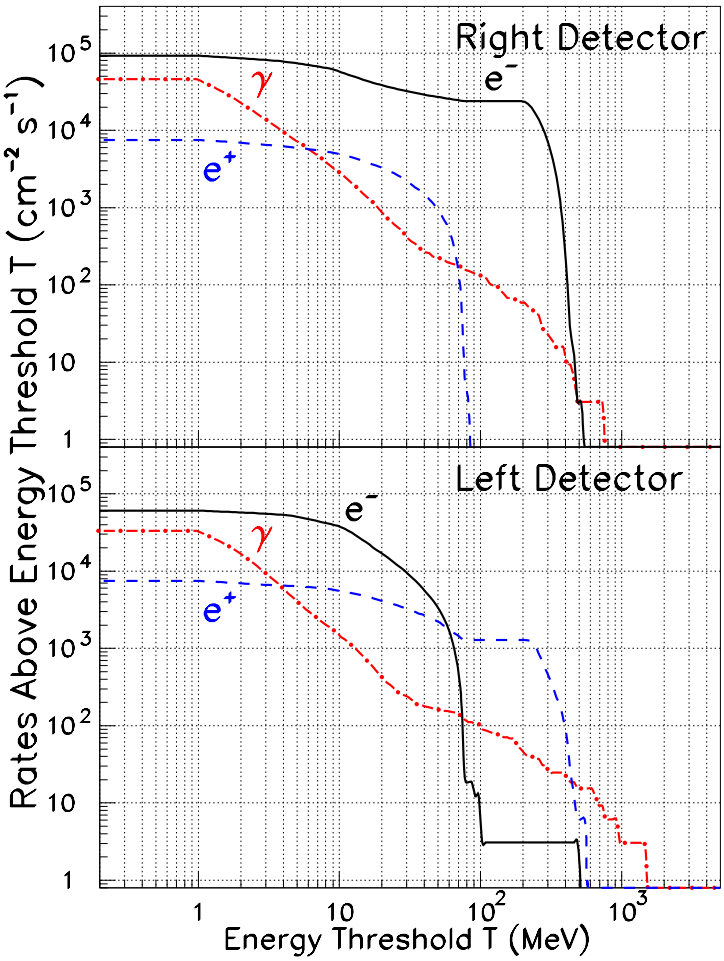

Figure 13: The background rates per unit area on each detector [17]. The simulation is based on a 4.8 GeV beam of 50 nA on a 5.0 cm NH_3 target, and a target field of 2.5084 T over an effective area of 16.74 inch in diameter.

detectors at large out-of-plane angles.

We plan to use an iron magnet to provide the necessary vertical and horizontal acceptance angles. Such a magnet was used by the University of Michigan's group in experiments at ANL's old ZGS[18] and the AGS at BNL[19]. This magnet has been in storage at BNL for 15 years and though a little dusty, appears to be in good shape. The power supply is in storage at the University of Michigan.

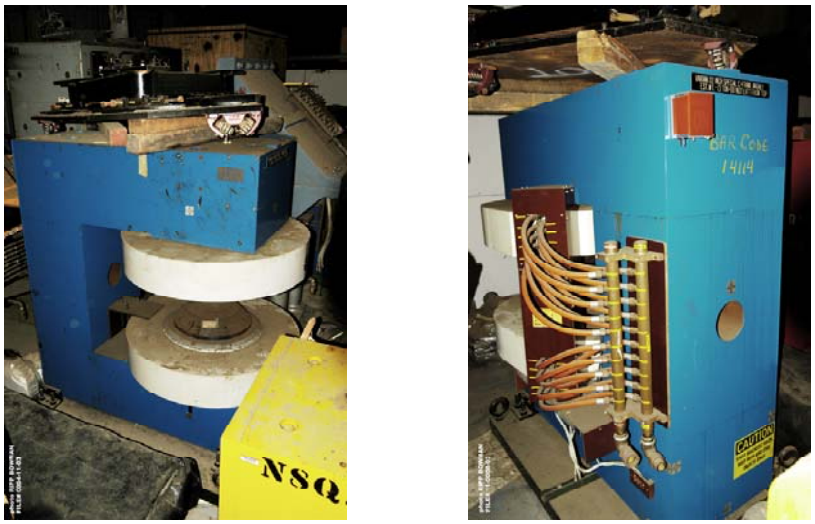

Figure 14: The 2.5 T magnet in storage near the AGS at Brookhaven, front view (left) and back view (right).

This type of magnet operates at 2.5 T and uses a horizontal refrigerator, in the case of the Michigan system a ^{3}He evaporation refrigerator. Because of the beam intensities expected on the target for this experiment, a ^{4}He evaporation refrigerator is needed. Two such refrigerators are available from the University of Virginia's polarized target lab. Operate the target only in one field direction with B-field downward, since changing the beam chicane to accommodate the change in target field direction would be impractical.

The 2.5 Tesla target magnet

The Michigan magnet has an open geometry of 270° in-plane and ±21° out-of-plane acceptance. The vertical opening is large enough such that the magnet pole face does not block the view of any detector. This open geometry allows flexibility for refrigerator and incident beam to come in from the backward direction. The shape of the magnet pole face is shown in Fig. 15. The excitation and uniformity curves of the Michigan magnet are shown in Fig. 16 and Fig. 17. The 75KW power supply used to obtain these data has a regulation

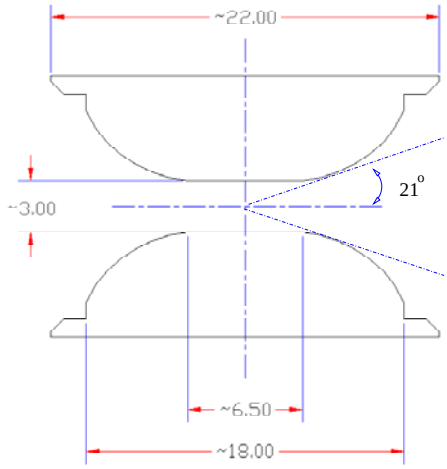

Figure 15: The pole face shape of the AGS target magnet. Units are in inches.

to the level of 1 part in 10^4. The magnet coils used for these data has been replaced with the original Varian coils at the start of of the AGS polarized target program. The magnet was originally used at ANL and then transferred to BNL where it was used in experiments for seven years.

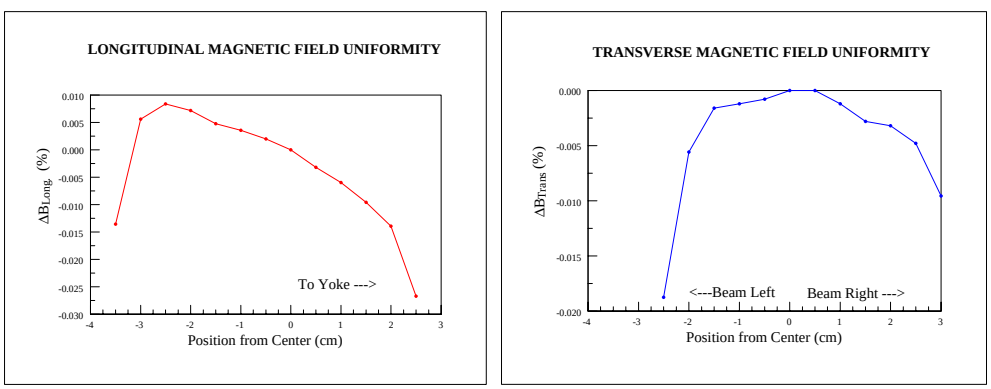

Figure 16: The target magnetic field uniformity in the direction along the beam (left pannel) and transverse to the beam (right pannel).

The ^{4}He Refrigerator

The refrigerator will be a horizontal one, of the Roubeau type [20] operating around 1K with a cooling power of about 1 watt with pumps such as those already used with polarized targets in Hall C. The schematic, from Roubeau's thesis, of this type of refrigerator is shown in Fig. 18. The refrigerator we intend to use is exactly like this and indeed was originally used at CERN in

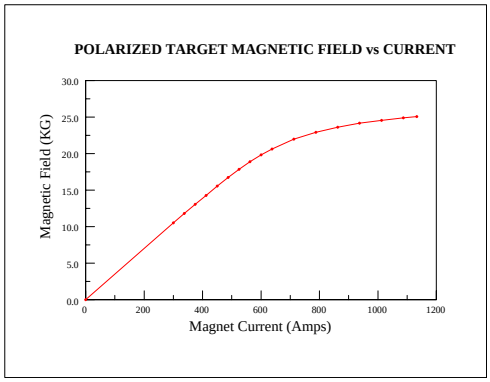

Figure 17: The target central magnetic field as a function of the current.

experiments. It has been refurbished and run at UVA in polarization tests. There is also a backup of similar design which has also been operated at UVA.

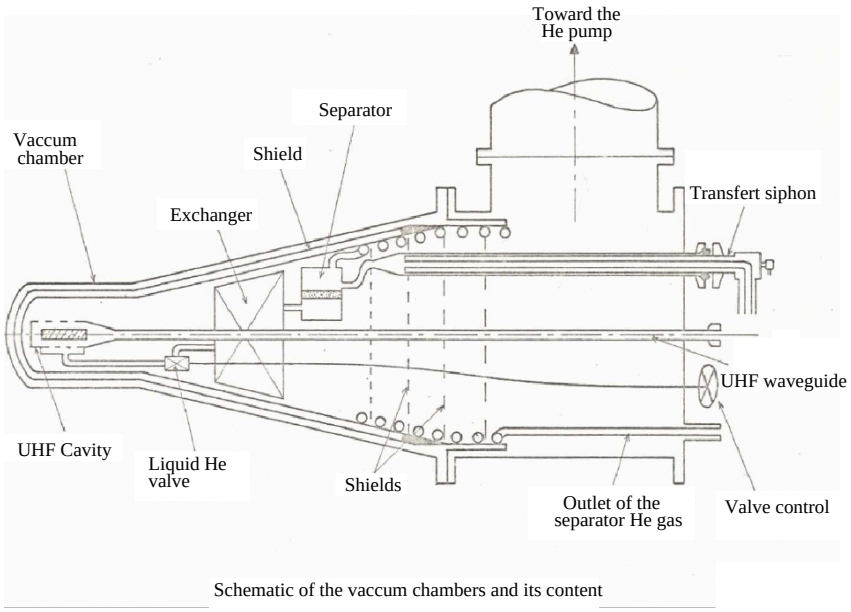

Figure 18: The ^{4}He refrigerator by P. Roubeau[20]. It was originally used at CERN in experiments, and has been refurbished and run at University of Virginia in polarization tests.

Target material

We intend to use irradiated NH_3 for the polarized target material. This is the best material for intense beams having a combination of the highest radiation resistance[21], very high polarization[22] and good dilution factor. Under the conditions of this experiment, maximum polarizations of about 45% are expected with an average of 38% being a reasonable expectation. The effects of radiation damage on the polarization have been well documented elsewhere[23,24].

It is not necessary to use ^{15}N ammonia for this experiment and so regular ammonia will be used and can be irradiated for use at the MIRF facility at NIST in Gaithersburg.

Microwaves and NMR

For a 2.5 T magnet, microwaves of frequency about 70 GHz are required. On hand are three vintage Carcinotrons, capable of up to 5 W power output, plus a power supply. However while these are appropriate for testing, they may not be suited for remote operation in a hostile environment for long periods. In particular the power supply cannot be remotely operated. It may be necessary to buy an EIO tube for high power operation and preserve the Carcinotrons for back up Remotely operable power supplies are on hand at JLAB and UVA . Devices for measuring power and frequency will also be necessary.

The target polarization has a fast build up time so it should be possible to reverse target polarization every six hours by changing microwave frequency. We will also anneal the target between each target flip. The time allocated for annealing the target, then flipping the spin and re-polarizing the target is 1.5 hours. The NMR system is available and needs little or no change, except a computer for DAQ.

3.8 Beam line

To maintain the target polarization, the beam has to be rastered. Rastering also insures uniform distribution of heat and radiation on the target material. We would use the slow rastering system developed for previous polarized target experiments in Hall C which produced a 2 cm diameter beam spot at the target. We would also plan to use the same Secondary Emission Beam Position Monitor (SEM) used in previous Hall C experiments.

The magnet field which is used to polarize the target will also bend the incoming and outgoing electron beam. In previous polarized target experiments, the target was polarized in the horizontal plane and the field direction was set so that the electron bend downwards. A series of chicane magnets was put in place to steer the beam and insure that the beam was bent up before entering the target field and therefore was horizontal at the target.

Obviously with the vertically polarized target field, the incoming and outgoing electron beams are bent in the horizontal direction. The existing chicane magnets would have to be rotated to bend the beam in the horizontal direction. The magnet for this experiment will be at 2.5 T with an effective diameter of 42.5 cm. The existing chicane magnets cannot compensate for the full beam deflection of the target field, but they can compensate for half of the deflection. If allowed the preferred solution would be to have a in-hall temporary beam dump. If this option is not feasible, then a bending magnet could be installed downstream of the target to bend the beam into the beam dump. Of course carefully consideration would have to taken to insure this downstream magnet does not become a secondary target illuminated by the

bremsstrahlung and produce large backgrounds in the hall. In either case, a helium bag would have to be used for the outgoing electron beam.

4 The Monte Carlo simulation

The existing Hall C Monte Carlo package, SIMC, was modified to have a vertical target field and include the calorimeters. For the present case, the target field was assumed to be uniform 2.5 T over a radius of 42.5 cm. When electrons were detected in the calorimeter, the position was determined by smearing with a Gaussian with a sigma of 0.4 cm and the energy was determined by smearing with a Gaussian with a sigma of $5\%/\sqrt{E}$. When protons were detected in the calorimeter, the position was set to the center position of the lead-glass block that was hit and it was assumed that there was no momentum information. When tracking back through the target field to determine the angles at the scattering vertex, the target position was assumed to be at the origin, since target position cannot be reconstructed. The particle velocity is needed for tracking back. For electrons, the energy determined from the calorimeter was used. For protons, proton momentum determined from the reconstructed electron angle and beam energy was used. The Monte Carlo was run for a 3 cm long target and 80 nA. To be able to run at a lower current of 50 nA we will run with a 5 cm long target. This will worsen the angular resolution shown in the following plots, but the angular resolution due to the protons still dominates since the length of the target seen by the detectors is reduced by $\sin(30^\circ)$. So the increase in the target length does not drastically effect the angular resolution.

In Fig. 19, results from the Monte Carlo for the $e+p$ elastic reaction (e going beam left) are plotted for: *Top plot:* the difference between the proton azimuthal scattering angles measured in the calorimeter and that predicted from the beam energy and the electron angle, *Middle plot:* the difference between the proton polar scattering angles measured in the calorimeter and that predicted from the beam energy and the electron angle and *Bottom plot:* the difference between the electron energy measured in the calorimeter and that predicted from the beam energy and the electron angle. Similarly, in Fig. 20, results from the Monte Carlo for the $p+e$ elastic reaction (p going beam left) are plotted for the difference in the azimuthal angles, polar angles and the electron energy. The resolution in the azimuthal angle is about 0.5° for both $p+e$ and $e+p$. While the resolution in the polar angle for $e+p$ is about 0.3° which is about twice as good as for the $p+e$ reaction.

5 Expected dilution factor

5.1 Determination using the Monte Carlo

The expected dilution factor from the quasi-free inelastic scattering from nitrogen and helium was calculated in the Monte Carlo assuming cross section from a model for ^{12}C. In Fig. 21, the top plot is the difference in the azimuthal

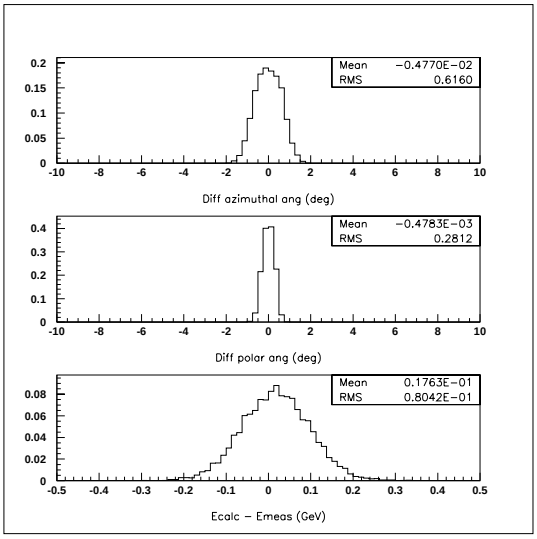

Figure 19: Plots of the results from the Monte Carlo for $e + p$ reaction. Plots are described in the text.

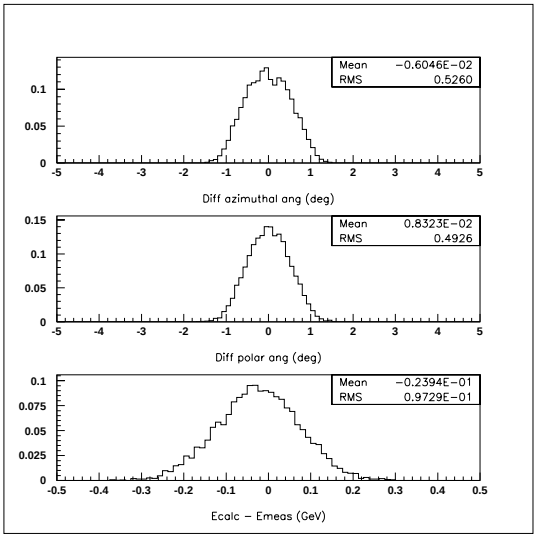

Figure 20: Plots of the results from the Monte Carlo for $p + e$ reaction. Plots are described in the text.

angle and the bottom plot is the difference in the polar angle for the $e + p$ reaction. The black line is the sum of the hydrogen plus helium and nitrogen contribution. The red line is only for the hydrogen and the blue line is only for nitrogen. In the top plot the green vertical line is a cut at $\pm 1.5^\circ$ on the azimuthal angle difference. With this alone the dilution factor is 72%. In the bottom plot of Fig. 21 is the difference in the polar angle with a cut of $\pm 1.5^\circ$ on the azimuthal angle difference. The black, red and blue lines have the same meaning as in the top plot. When an additional cut of $\pm 1.5^\circ$ is placed on the difference in the polar angle then the dilution factor increases to 89%. In Fig. 22, the top plot is the difference in the azimuthal angle and the bottom plot is the difference in the polar angle for the $p + e$ reaction. The histograms in the top and bottom plots have the same meaning as describe for Fig. 21. Again, in the top plot the green vertical line is a cut at $\pm 1.5^\circ$ on the azimuthal angle difference. With this alone the dilution factor is 73%. When an additional cut of $\pm 1.5^\circ$ is placed on the difference in the polar angle then the dilution factor increases to 91%. Of course this Monte Carlo only contains the quasi-free inelastic contribution and one may ask about the other inelastic contributions. This issue is addressed in the next subsection, by looking directly at data taken in Hall B with a polarized target.

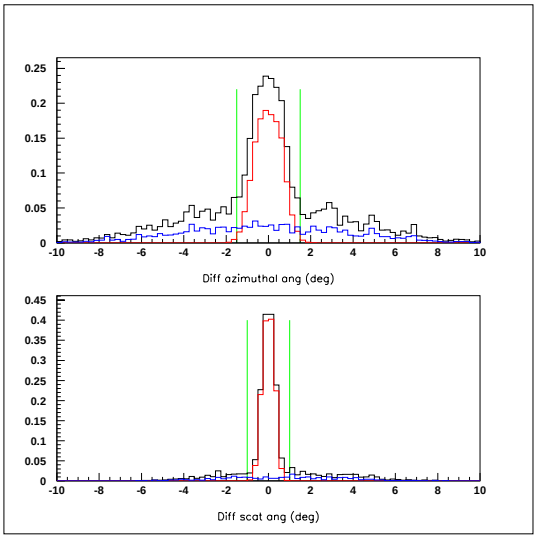

Figure 21: Plots of the results from the Monte Carlo for $e + p$ reaction. Details given in the text. In the bottom plot, the "scat ang" is the polar angle.

5.2 Determination using CLAS data

In order to check that the angular correlation cuts we propose will be sufficient to isolate *ep* elastic events with less than 10% contamination from backgrounds, we have studied data from the Eg1 experiment in Hall B. This experiment used an NH3 target similar to that of this proposal, an electron beam with energy of 5.7 GeV, and a current of 5 nA. The advantages of

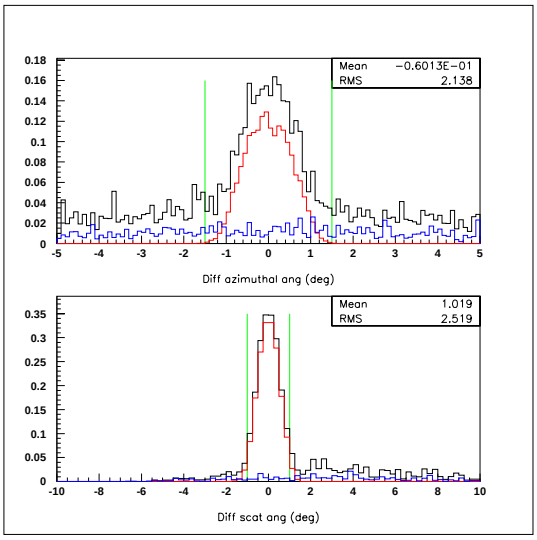

Figure 22: Plots of the results from the Monte Carlo for $p + e$ reaction. Plots are described in the text. In the bottom plot, the "scat ang" is the polar angle.

using actual data (compared to our simulation), is that inelastic scattering is included, and electron-pion coincidences are included as well as electron-proton events (since we will not be able to distinguish protons and pions in our detector).

From a typical run with the torus polarity set to bend electrons outwards, we selected pairs of charged particles which satisfied the following criteria:

- $20 < \theta < 36$ degrees
- one particle had an energy deposit in the electromagnetic calorimeter of at least 2 GeV (electron candidate), and the other particle had an energy deposit of less than 2 GeV (hadron candidate)
- $W < 2$ GeV, where W is the invariant mass as reconstructed from the electron angle and momentum
- hadron momentum greater than 0.5 GeV (to simulate the effects of the target field which will tend to sweep out low momentum hadrons)

No cuts on particle charge where made (since this won't be known in our experiment), and the Cherenkov information was ignored (although a small Cherenkov signal was required in the main hardware trigger, which tends to remove events with no electrons). Fig. 23a,d,g show the distributions in W of the electron (as determined from the tracking), the difference in actual hadron angle from that predicted from the electron angle and known beam energy ($\delta\theta$), and the difference in azimuthal angles ($\delta\phi$) with no additional cuts applied. Applying a ± 1 degree cut in $\delta\theta$ is already enough to reduce the non-elastic background in the $\delta\phi$ distribution from about 80% to about 20% (compare Fig. 23g and 23h), and make the elastic peak clearly visible in the W distribution (see Fig. 23b). Adding a cut $W < 1.3$ GeV (the W

resolution in this proposal will be about ± 0.25, so this is fairly realistic), reduces the background in the $\delta\phi$ distribution to less than 10%, as predicted by our simulation. This can also be seen in Fig. 23c, which includes not only the $\delta\theta$ cut, but also a ± 2 degree cut in $\delta\phi$.

We conclude that with the calorimeter energy and position resolutions of our proposed detector, we will have a background to *ep* elastic events of less than 10%.

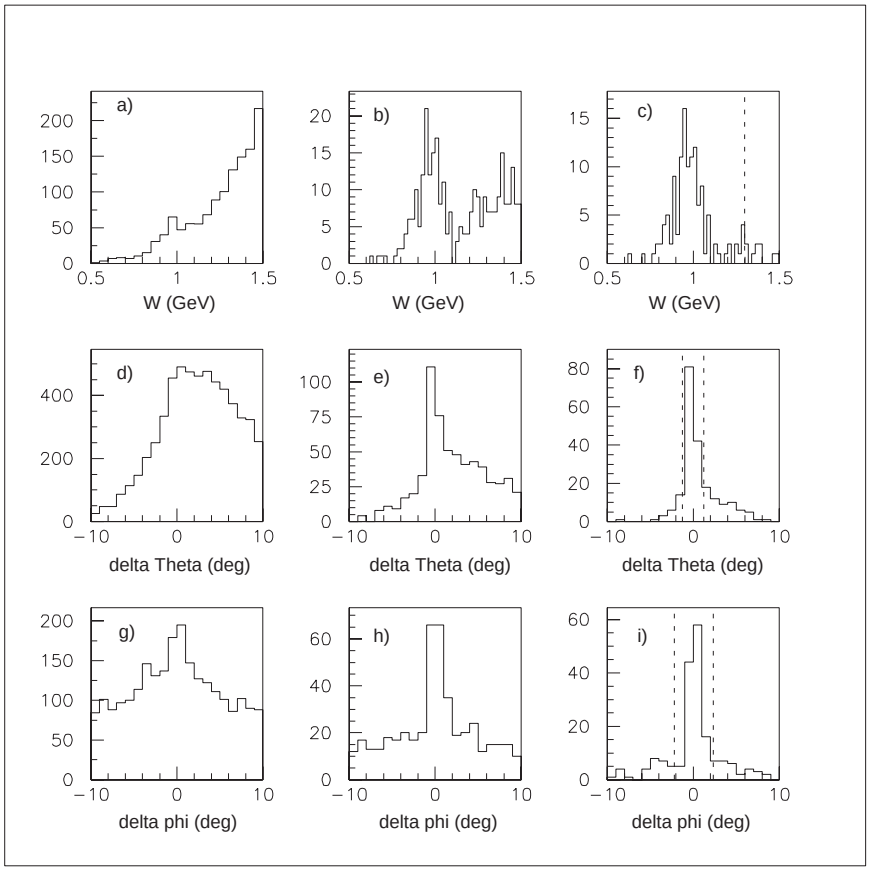

Figure 23: From CLAS data similar to this proposal, the distributions in W for: a) no cuts; b) with a ± 1 degree cut in $\delta\theta$; c) with also a ± 2 degree cut in $\delta\phi$. Distributions in $\delta\theta$ are shown for: d) $W < 2$ GeV; e) and a ± 2 degree cut in $\delta\phi$; f) with also $W < 1.3$ GeV. Distributions in $\delta\phi$ are shown for: g) $W < 2$ GeV; h) and a ± 1 degree cut in $\delta\theta$; f) with also $W < 1.3$ GeV.

6 Systematic uncertainties

6.1 Cross checks on A_y and the systematic uncertainties

A clear observation of A_y must pass the test of the following cross checks, which are built-in within the same data set. Data from all Q^2 bins will be combined to perform these tests.

- A_y from two independent DAQ should agree. Two combination of detector sections, the left-upper+ right-lower and left-lower+right-upper combinations, should yield the same A_y within statistics.
- A_y obtained from $e+p$ type coincidence events should change sign compared to A_y obtained from $p+e$ type events.
- The relative luminosities obtained from different units of Lumi-detector should be consistent.
- When the sign of target spin in each time slot is randomly assigned, A_y should be average to zero.

Physics single-spin asymmetries originated from the pion production channels should contribute a negligible amount to our A_y results. As demonstrated in the analysis of Hall B eg1 data, a cut on W will eliminate most of possible contamination events from pion production channels. The energy resolution of our calorimeter is good enough to allow such a cut on W.

For each of the above cross checks, we will have enough statistics in the data to check consistency to within 0.1%. Therefore, the unknown systematic uncertainties in this experiment should be less than 0.1%.

6.2 Correction on A_y due to target polarization drifts

The target polarization between spin up and spin down runs does not have to be exactly the same. A drift in the target polarization does not cause any single-spin asymmetry to start with, it only results in a small change which is easy to correct. Assuming the yield is: $\sigma = \sigma_0 + P_T\sigma_1$ for target spin up and spin down, we have: $\sigma_+ = \sigma_0 + P_T\sigma_1$ and $\sigma_- = \sigma_0 - P_T\sigma_1$. The measured asymmetry is:

$$A_0 = \frac{\sigma_+ - \sigma_-}{\sigma_+ + \sigma_-} = P_T\frac{\sigma_1}{\sigma_0}. \tag{11}$$

If during spin down runs the average target polarization changes to $P_T + \delta P_T$, such that $\sigma'_+ = \sigma_0 + P_T\sigma_1$ and $\sigma'_- = \sigma_0 - (P_T + \delta P_T)\sigma_1$, the measured asymmetry changes to:

$$A' = \frac{\sigma'_+ - \sigma'_-}{\sigma'_+ + \sigma'_-} = A_0\frac{1 + \dfrac{\delta P_T}{2P_T}}{1 - \dfrac{\delta P_T}{2P_T}\cdot A_0}. \tag{12}$$

Since $A_0\delta P_T/2P_T \ll 1$, we have:

$$A' \approx A_0(1 + \frac{\delta P_T}{2P_T})(1 + \frac{\delta P_T}{2P_T}\cdot A_0) \approx A_0(1 + \frac{\delta P_T}{2P_T}). \tag{13}$$

As long as the target polarization is under continuous monitoring by NMR, the drifts in average polarization between spin up and spin down runs will not cause any significant uncertainty in A_y.

7 Beam time request

The beam time request is listed in detail in Table 4. We request 480 hours (20 days) of beam time in total, of which 360 hours is for beam on the polarized target. A large amount of overhead time (120 hours total) is requested. Much of this time is for polarization reversals, estimated to take 1.5 hours after every 6 hours of beam on target. In addition, the target material will be changed about 3 times during the experiment. Includeing time for the TE measurements, target material changes will typically take several shifts which in most case can coincide with the scheduled accelerator maintenance time. The requested beam energy is 4.8 GeV. Beam polarization is not a concern for the A_y measurement. If polarized beam is available, double-spin asymmetry measurements can be performed at the same time as a by-product.

Beam on polarized NH_3 target	**360**
Target overhead, detector checks and unpolarized target runs	**120**
Total Time Requested	**480 (20 days)**

Table 4: Beam time request.

8 The Expected Results

From the measured asymmetry $\mathcal{A}_{measure}$ the physics asymmetry of A_y can be obtained after corrections for the target polarization and the dilution factor:

$$A_y = \frac{\mathcal{A}_{measure}}{P_T \cdot \eta} \tag{14}$$

The expected statistical uncertainties on A_y are shown in Fig. 24, as a function of the scattered electron's center of mass angle θ^e_{cm}. The expected accuracies are compared with the SLAC-1970 experiment in Fig. 25 as a function of Q^2. The two low-Q^2 (low θ^e_{cm}) points are from the proton-singles measurement of spectrometer and the electron singles measurement of the 10° Lumi units, respectively. For the high Q^2 points, the statistical error is determined by combining events from both $e+p$ type and $p+e$ type coincidence. The error are listed in Table

This experiment can clearly identify a non-vanishing A_y. Although the predictions of the inelastic intermediate state contribution are model dependent, the predictions of elastic contribution agree from different calculations. Different models also tend to agree that the full size of A_y can only be larger than the elastic contribution alone.

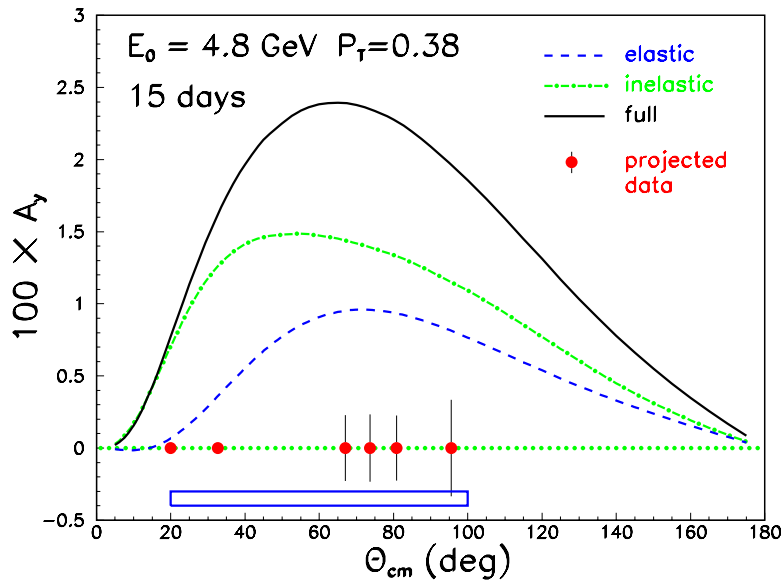

Figure 24: The expected statistical uncertainties of A_y at $E_0 = 4.8$ GeV, as a function of θ_{cm}, the center-of-mass scattering angle, compared with calculation of A. Afanasev *et al.*

9 Relation with other experiments

- Hall C G_{Ep}-III. This experiment will use the same calorimeter blocks as in the G_{Ep}-III experiment. The same group of people will be collaborating in the two experiments. Re-stacking of the lead glass array, needs careful planning and new patch panels would have to be built. The electronics and HV planned for G_{Ep}-III can be used for this experiment, but they were have to be an obvious rearrangement of the electronics.
- Other polarized target experiment in Hall C. The four calorimeter array sectors, splitted from the original geometry, can be put back together into one large array. This will not affect the approved SANE experiment, the flavor decomposition proposal, proton transversity LOI and the exclusive channel single-spin asymmetry LOI. An initial study has started to design a superconducting magnet that can provide 5.1 T field for a vertically polarized target system. Such a target will provide 80% proton polarization for future transversity experiments at 6 and 12 GeV. While this direction is being actively pursued by members of this collaboration, the technical challenges in the design and development stage of the superconducting magnet are not expected to be overcome in a short time scale.

10 Summary

We propose to measure the target single-spin asymmetry A_y in elastic $ep^{\uparrow} \rightarrow ep$ reaction at Hall C using a vertically polarized NH_3 target. The single-spin

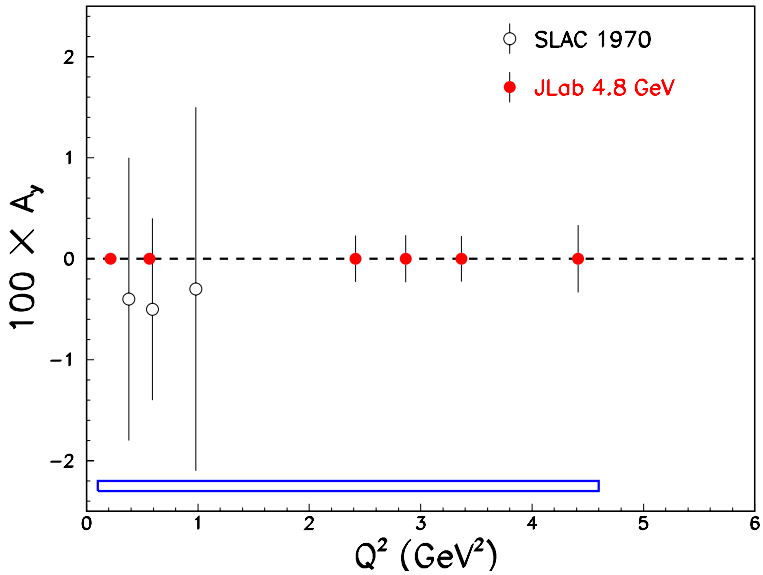

Figure 25: The expected statistical uncertainties of A_y as a function of Q^2, compared with the SLAC measurement. Note that the SLAC data were taken in the range of $13.5° < \theta_{cm} < 19.9°$ where A_y is suppressed by a kinematic factor of $\sin\theta_{cm}$ (see Fig. 24).

asymmetry A_y is sensitive to the imaginary part of the two-photon exchange amplitude. Four identical lead glass arrays will be used to detect electron and proton in coincidence. Both $e+p$ type and $p+e$ type coincidence events will be collected simultaneously. Several independent methods will be used to determine relative luminosities. A total of 20 days of beam time is requested at 4.8 GeV beam energy.

References

1. L. Andivahis *et al.*, Phys. Rev. D **50**, 5491 (1994).
2. M.K. Jones *et al.*, Phys. Rev. Lett. **84**, 1398 (2000).
3. O. Gayou *et al.*, Phys. Rev. Lett. **88**, 092301 (2002).
4. A summary of the existing data can be found in J. Arrington, nucl-ex/0305009.
5. Jefferson Lab experiment E01-001, J. Arrington, R.E. Segel, *et al.*
6. M.E. Christy *et al.*, to be submitted to Phys. Rev. C.
7. P.A.M. Guichon, M. Vanderhaeghen, hep-ph/03060007 and PRL.
8. P.G. Blunden, W. Melnitchouk, J.A.Tjon, nucl-th/0306076 and PRL.
9. A. De Rujula, J.M. Kaplan and E. De Rafael, *Nucl. Phys.* B **53**, 545 (1973).
10. A. Afanasev, I. Akushevich, N.P. Merenkov, hep-ph/0208260.
11. T. Powell *et al.*, *Phys. Rev. Lett.* **24**, 753 (1970).
12. J. Gunion and L. Stodolsky, *Phys. Rev. Lett.* **30**, 345 (1973)
13. R. Blankenbecker and J. Gunion, *Phys. Rev.* D **4**, 718 (1971)

14. M.N. Rosenbluth, Phys. Rev. **79**, 615 (1950).
15. M.L. Goldberger, Y. Nambu and R. Oehme, Ann. of Phys. **2**, 226 (1957).
16. J. Mar, *Phys. Rev. Lett.* **21**, 482 (1968).
17. P. Degtiarenko, private communications, November 2003.
18. D. G. Crabb et al., Phys. Rev. Lett. 41, 1257 (1978)
19. G. R. Court et al., Phys. Rev. Lett. 57, 507 (1986)
20. M. Borghini et al., Nucl Instr. & Meth., 49, 248 (1967) and49, 259 (1967)
21. D. G. Crabb and W. Meyer, Ann. Rev. Nucl. Part. Sci. 47, 67 (1997)
22. D. G. Crabb et al., Phys. Rev. Lett., 64, 2627 (1990)
23. C. Harris, Proc. Int. Workshop on Pol. Sources and Targets (PST99), University of Erlangen-Nürnberg, eds., A Gute, S. Lorenz and E Steffens 1999, p. 410.
24. D. G. Crabb and D. B. Day, Nucl. Instr. and Meths., A356, 9 (1995)